Charge Transfer at Junctions of a Single Layer of Graphene and a Metallic Single Walled Carbon Nanotube

Geraldine L. C. Paulus, Qing Hua Wang, Zachary W. Ulissi, Thomas P. McNicholas, Aravind Vijayaraghavan, Chih-Jen Shih, Zhong Jin, and Michael S. Strano*

Junctions between a single walled carbon nanotube (SWNT) and a monolayer of graphene are fabricated and studied for the first time. A single layer graphene (SLG) sheet grown by chemical vapor deposition (CVD) is transferred onto a SiO$_2$/Si wafer with aligned CVD-grown SWNTs. Raman spectroscopy is used to identify metallic-SWNT/SLG junctions, and a method for spectroscopic deconvolution of the overlapping G peaks of the SWNT and the SLG is reported, making use of the polarization dependence of the SWNT. A comparison of the Raman peak positions and intensities of the individual SWNT and graphene to those of the SWNT-graphene junction indicates an electron transfer of 1.12×10^{13} cm^{-2} from the SWNT to the graphene. This direction of charge transfer is in agreement with the work functions of the SWNT and graphene. The compression of the SWNT by the graphene increases the broadening of the radial breathing mode (RBM) peak from 3.6 ± 0.3 to 4.6 ± 0.5 cm^{-1} and of the G peak from 13 ± 1 to 18 ± 1 cm^{-1}, in reasonable agreement with molecular dynamics simulations. However, the RBM and G peak position shifts are primarily due to charge transfer with minimal contributions from strain. With this method, the ability to dope graphene with nanometer resolution is demonstrated.

1. Introduction

Single layer graphene (SLG) is a planar sheet of sp^2-bonded carbon atoms, organized into a hexagonal crystal lattice. It is a semi-metal or zero-band gap semiconductor.[1–3] A single walled carbon nanotube (SWNT) can be thought of as a single layer of graphene rolled into a seamless hollow cylinder with a diameter on the nanometer length scale and electronic properties that vary from metallic to semi-conducting depending on its diameter and chiral angle.[4–6] Both materials have exceptional optical, mechanical, thermal and electronic properties.[1–6]

Although electronic transport in graphene as well as in SWNTs has been extensively explored,[7–10] very few studies have investigated transport through the interface formed between a carbon nanotube and graphene or graphite, and in fact no study to date has investigated a junction between SWNTs and SLG. Paulson et al. used conductive atomic force microscopy (AFM) to measure the contact resistance between a multi-walled carbon nanotube (MWNT) and highly ordered pyrolytic graphite (HOPG) and found that the resistance varies significantly (between ~5 and ~75k Ω) based on the orientation of the MWNT lattice with respect to the graphite lattice.[11] Both HOPG and MWNT are considered to be zero-gap metals. Pei et al. grew both semiconducting (sc-) and metallic (m-) SWNTs on top of exfoliated few-layer-graphene (FLG) and designed a bottom-gated

G. L. C. Paulus, Dr. Q. H. Wang, Z. W. Ulissi,
Dr. T. P. McNicholas, C.-J. Shih, Dr. Z. Jin,
Prof. M. S. Strano
Department of Chemical Engineering
Massachusetts Institute of Technology
Cambridge, Massachusetts 02139, USA
E-mail: strano@mit.edu

Dr. A. Vijayaraghaven
School of Computer Science
University of Manchester
Manchester, M13 9PL, UK

field-effect transistor (FET) by contacting the SWNTs and the FLG with palladium electrodes.[12] They observed fairly symmetric *I–V* curves for a junction between a m-SWNT and FLG, suggesting no obvious potential barrier exists between the m-SWNT and graphene. For a sc-SWNT/FLG junction they observed rectifying behavior, characterized by a small positive threshold voltage of 0.1 V, indicating the existence of a Schottky barrier.

In this work, we create and study a junction between SWNTs and a monolayer of graphene, an ideal one-dimensional-to-two-dimensional carbon-allotrope conductive interface, for the first time. Our interest is in the degree of charge transfer (i.e. doping) between both materials. The ability to controllably dope graphene and change its work function is key to its implementation in devices such as (opto-) electronics and biosensors, and interconnects.[13–17] Additionally, there is a strong preference to dope graphene without covalently functionalizing it or substituting carbon atoms, such that graphene's outstanding electronic properties are preserved.[18,19] Finally the transition from 2D to 1D electronic conduction may lead to new physics that could be of interest for engineering novel electronic junctions, including rectifiers, transistors and sensors. The interactions between a single m-SWNT and a single layer graphene sheet that covers the SWNT are studied using Raman spectroscopy, revealing that the SWNT locally dopes the graphene. We demonstrate polarized spectral deconvolution of the Raman spectra as a technique to enable the study of these carbon junctions. A molecular dynamics simulation rules out strain as the cause of the observed Raman peak shifts. Since the SWNT is able to dope the graphene in a spatially controlled way without affecting its sp^2-lattice structure, we do not expect a significant mobility loss in the graphene. Moreover, it is now possible to dope graphene with nanometer precision.

2. Results

Aligned SWNTs were grown on a SiO_2/Si wafer via chemical vapor deposition (CVD). A monolayer of graphene was also synthesized via CVD and transferred on top of the wafer with SWNTs as described in the Experimental Section. **Figure 1** shows a schematic of the SWNT/graphene junction. Figure S1 (Supporting Information) shows an array of scanning electron microscopy (SEM) images of the entire wafer and indicates the particular SWNT/graphene junction being investigated, as well as an AFM image of a representative SWNT. The way the sample is made allows for direct comparison between different regions of the same sample. Raman spectroscopic maps were taken at 3 different regions in the same sample (Figure 1). In Region 1, 75 spatially distinct Raman spectra were collected along ~100 μm of the bare SWNT. In Region 2 (~20 × 100 μm), 75 spatially distinct Raman spectra are taken of the graphene alone. Finally we were able to gauge the influence of the SWNT on the graphene and vice versa by collecting 75 Raman spectra in distinct locations in Region 3 where the graphene covers the SWNT (spectra of the junction were taken for ~100 μm along the length of the SWNT). This allows for direct internal controls. The reason
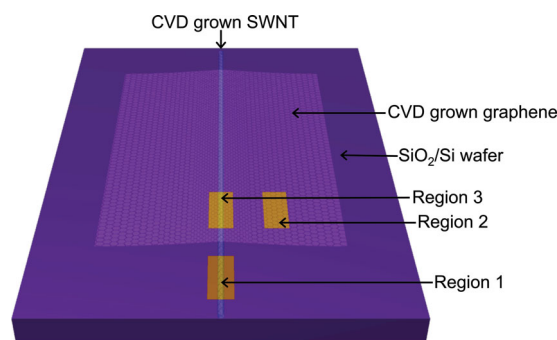

Figure 1. Schematic of the SWNT-CVD graphene junction (not to scale). Region 1 indicates a part of the SWNT that is not covered by graphene (Raman spectra taken along ~100 μm of the SWNT). Region 2 indicates a (~100 μm by 20 μm) region of graphene away from the junction. Region 3 indicates a region where the graphene is directly on top of the SWNT (Raman spectra taken along ~100 μm of the SWNT). In order to obtain statistically relevant data, in each region 75 distinct Raman spectra were collected at different spots. Given a laser spot size of ~1 μm, the spectra were taken at least 1.25 μm apart from one another, thereby avoiding overlap.

for collecting this many spectra in each region is the ability to take into account any possible spatial inhomogeneity of the graphene, SWNT and the substrate and to make meaningful statistical comparisons between the different regions.

Figure 2 shows representative Raman spectra from each of the different regions. Figure 2(a) is a representative spectrum of the SWNT used for this study in Region 1. The characteristic Raman modes of SWNTs are the RBM (radial breathing mode), which typically occurs between 100-300 cm⁻¹; the G band at ~1580 cm⁻¹; the D peak (1300-1400 cm⁻¹) and the 2D peak (2600-2800 cm⁻¹).[20] By locating the RBM of the investigated SWNT (177 cm⁻¹) and the laser energy (1.96 eV) on a Kataura plot,[21] we assign the SWNT as metallic, and most likely a (13,7) chirality SWNT, with a diameter of ~1.35 nm. Due to the curvature of the SWNT, the G peak splits into two components G⁻ (at 1572 cm⁻¹) and G⁺ (at 1592 cm⁻¹). Figure 2(b) shows the graphene Raman spectrum. A monolayer of graphene is typically characterized by a D-peak near 1300–1350 cm⁻¹, a G-peak near 1580 cm⁻¹ and a 2D peak near 2600–2700 cm⁻¹.[22,23] The relative intensities and the widths of the G and 2D peaks as well as the color contrast in the optical microscopy image confirm we have grown monolayer graphene (SLG).[22,23] A more detailed analysis of the SWNT and graphene Raman signature is included in the Supporting Information, Section II.

Figure 2(c) shows a representative spectrum of graphene covering the SWNT. The RBM feature of the SWNT and the 2D feature of graphene are clearly distinguishable; however, the G-bands of the SWNT and the graphene overlap, making it difficult to tell which of the G-peaks is characteristic of the SWNT and which of the graphene. Because the Raman signal of a SWNT depends on the laser-polarization, mainly due to its anisotropic shape,[24–26] it can be blocked while maintaining the signal from the graphene by rotating the polarization angle of the incident laser beam. **Figure 3** shows the laser-polarization-dependence of the Raman signal of the SWNT and the graphene, obtained by using a half-wave plate
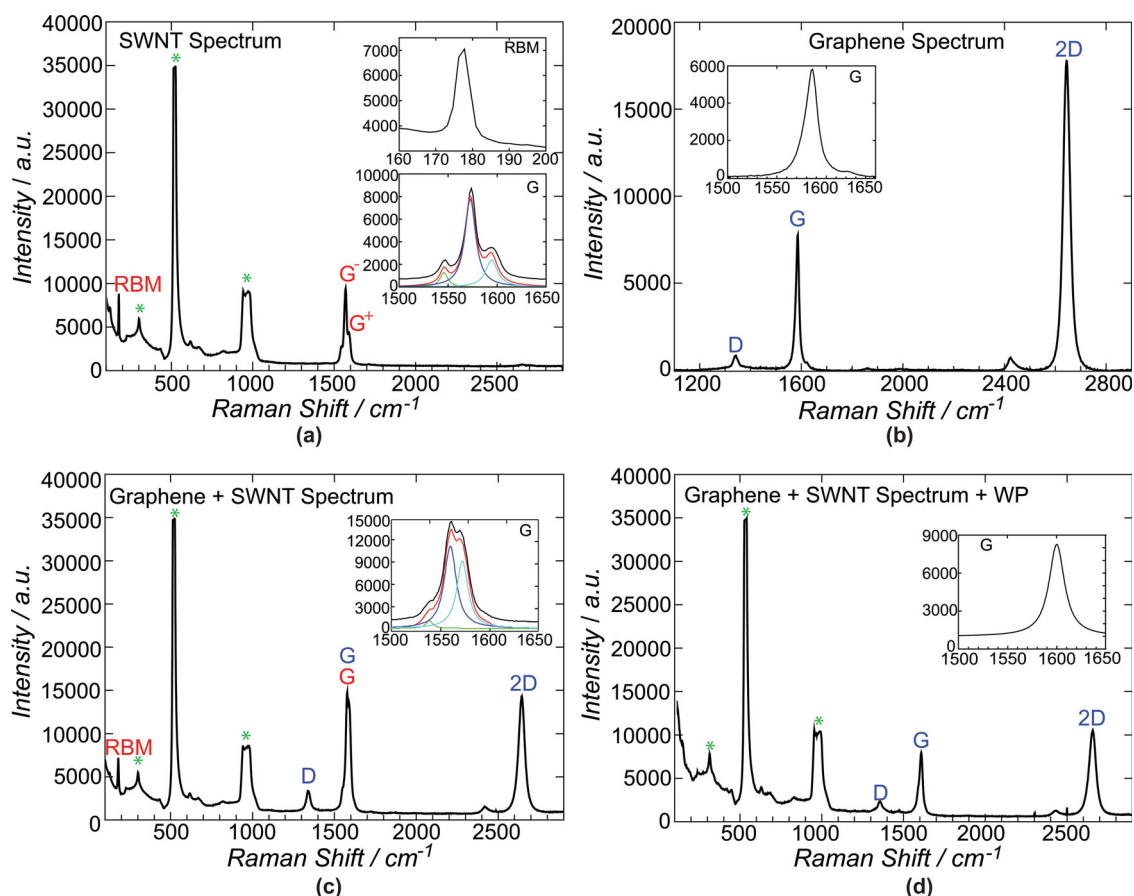
Figure 2. Representative Raman spectra, taken at 633 nm laser excitation, with the characteristic peaks assigned (SWNT peaks denoted in red, graphene peaks in blue and substrate peaks with green asterisks). (a) Spectrum taken in Region 1 (SWNT exposed to air). The two insets show the RBM and the G peak. (b) Spectrum taken in Region 2 (Graphene exposed to air). Inset shows the G-peak. (c) Spectrum taken in Region 3 (Graphene covering SWNT). Inset shows the G-peaks. (d) Spectrum taken in Region 3 with a half-wave plate that ensures the laser polarization is perpendicular to the SWNT. Inset shows the G-peak.

to rotate the incident polarization. The intensity of the Raman signal is the largest when the polarization of the incident light is parallel to the nanotube axis ($\alpha = 0°$ and $\alpha = 180°$) and disappears completely when it is perpendicular to the nanotube axis ($\alpha = 90°$, Figure 3(a)). For the SWNT the polarization difference ratio $\Pi = \frac{I_{0°} - I_{90°}}{I_{0°} + I_{90°}}$ (where I represents the intensity of the signal, measured as the area under the curve), equals 0.98. It is important to verify the effect of the half-wave plate on the Raman signal of graphene, shown in Figure 3(b); the half-wave plate has no influence on the G-peak position and very little on the G-peak intensity ($\Pi = -0.04$). This result is expected, since graphene is largely isotropic. Figure 2(d) shows the spectrum taken at the exact same location as the one in Figure 2(c) but with the insertion of the half-wave plate at $\alpha = 90°$. The RBM and G-band signals of the SWNT disappear whereas the graphene peaks are still present.

Figure 4 and Figure S2 show the influence of the SWNT on the CVD-graphene by comparing the different data points in Region 2 to those in Region 3. The datasets presented here, as well as those in **Figure 5** and **Figure 6**, clearly show the importance of collecting multiple spectra in each region and comparing the different distributions as a whole. Each distribution shows some spread. This is possibly due

to small temperature and humidity fluctuations throughout the experiment and small spatial variations in doping (e.g. residual PMMA on the graphene). We note though that all the shifts between the different distributions shown in Figures S2, and Figures 4, 5 and 6 are statistically significant, according to both the student t-test and the Kolmogorow-Smirnov test (where the likelihood that the two sample sets belong to the same population was virtually 0 for all datasets).

The G and 2D peaks contain information about the level of doping and strain in graphene.[22,23,27–29] Figure S2(a) shows how the G-peak position of graphene upshifts by about 10 cm^{-1} when it covers the SWNT, indicative of doping. The 2D peak decreases by ~3 cm^{-1} (Figure S2(b)), which indicates that the type of doping is n-type.[29] Figure 4(a) shows the 2D peak position versus the G peak position of graphene on the SiO$_2$ substrate (black squares) and on top of the SWNT (red dots). The dashed lines represent the doping trajectories adapted from existing literature: Das et al. injected excess charge carriers in graphene via electrostatic gating while simultaneously recording the graphene Raman signal.[29] The curves are shifted to account for the dependence of the 2D peak position on excitation laser wavelength since the original trajectories by Das et al. were collected
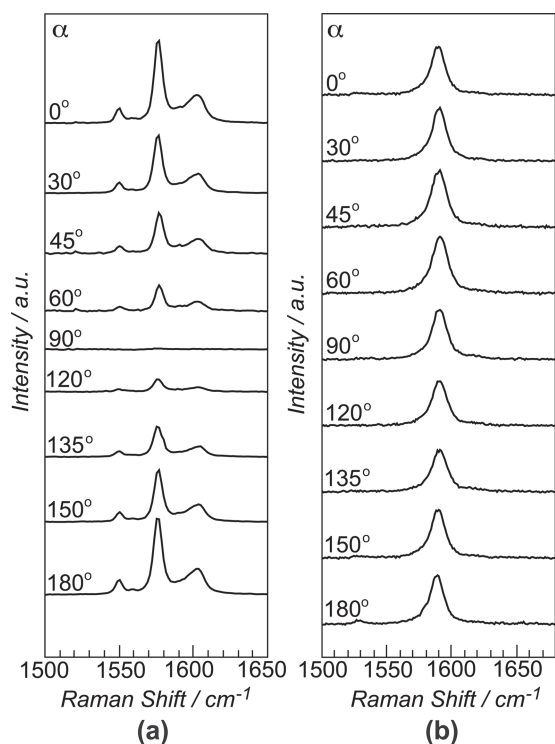
Figure 3. Influence of a half-wave retardation plate on the G-band Raman signal of (a) SWNT and (b) graphene. α represents the angle between the polarization of the excitation laser and a line parallel to the SWNT.

at 532 nm and in this work a 633 nm excitation source was used.[29] The trajectory starts out on the left side of the graph with undoped graphene. For both p- and n- doping the G peak position increases but the 2D position shifts differently for each type of doping resulting in the two branches in Figure 4(a). Our data superimposed on these doping trajectories also supports the conclusion of n-doping of graphene from the m-SWNT.

Another measure of doping is a decreased 2D/G intensity ratio,[27,29,30] depicted in Figure S2(d). Combined with the previous trend of increased G peak, another doping trajectory can be set up (Figure 4(b)). It should be noted that G-peak information of graphene on top of the SWNT was deduced from spectra taken with the half-wave plate, as it is clear from Figure 2(c) it is hard to deduce which peaks belong to graphene and which to SWNT without it. Due to the introduction of the additional optics the intensity of the G-peak decreases by ~8.5% (see Figure S3) and it can be considered as the lower limit of the actual value of the G peak intensity. This implies that the 2D/G intensity ratio in Figure 4(b) and S2(d) for graphene on top of the SWNT is an upper limit, which further confirms the doping trend.

A final indication doping is a decrease of the G peak full width at half maximum (FWHM),[27,29,30] which we also observe (Figure S2(c), Figure 4(c)). Figure 4(c) shows the FWHM of the G peak plotted against the G peak position. The dashed doping trajectory, adapted from [29] indicates increased doping levels lead to a stiffer G peak and an increased G peak position. This trend line has been
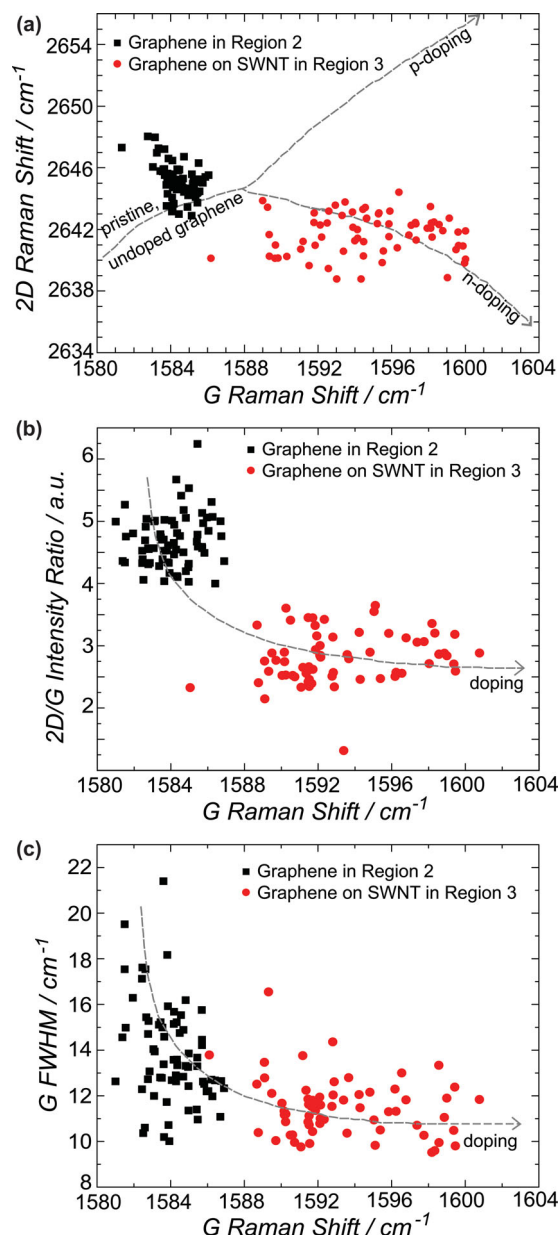

Figure 4. Influence of the SWNT on the graphene. Comparison of some characteristic Raman signals of the graphene in Region 2 (on the substrate, black squares) and Region 3 (on top of the SWNT, red dots). (a) Effect of SWNT on the G and 2D-peak position of graphene. (b) Effect of the SWNT on the 2D/G intensity ratio and the G position of graphene. (c) Effect of the SWNT on the G peak position and width of the graphene. Dashed lines are trendlines that represent doping trajectories adapted with permission from [29] and [58].

shifted upward to take into account the larger G peak FWHM in CVD graphene, compared to that in exfoliated graphene.

Note that the G peak position data taken in Region 3, shown in Figures 4 and S2 are characterized by a slightly broader distribution than the other distributions. This is likely because the SWNT G peak and the graphene G peak in Region 3 partially overlap and the deconvolution slightly overestimates the width of the graphene G peak.
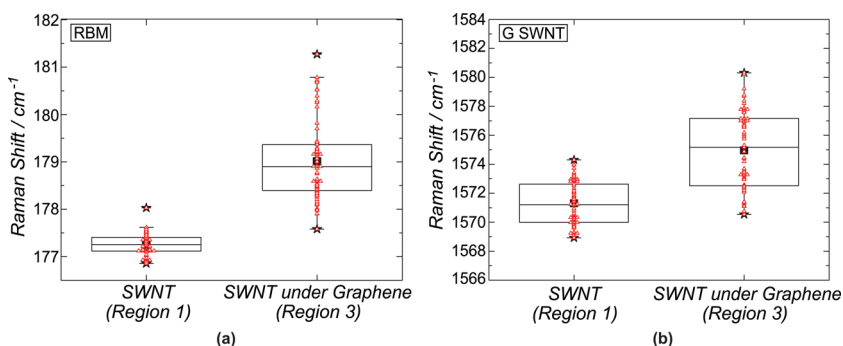
(a)

(b)

Figure 5. Influence of the graphene on the SWNT peak positions. Comparison of Raman signals of the graphene in Region 1 (exposed to air) and Region 3 (underneath the graphene). The lower and higher ends of the boxplots represent the 25 and 75 percentile marks of the distributions respectively, and the middle line is the median value. Minimum and maximum values are represented by black stars, and the average is the black square. The red triangles in (a),(b) represent the complete dataset superimposed on the boxplots.

both the RBM and the G peak position of the SWNT when it is covered by graphene. It has been shown both theoretically and experimentally that upon doping the RBM and G-peaks of SWNTs can upshift.[31–36] There is some disagreement in the literature about the exact nature and extent of this doping. Farhat et al. claim the RBM upshift is only observed for m-SWNTs,[31] whereas others do not make the distinction between sc-SWNTs and m-SWNTs when observing this phenomenon.[33,36] The experimental conditions and nanotube sources are different in each publication. Since Farhat et al. also use CVD-grown SWNTs, their observations may be more relevant to our work.

Comparing the SWNT Raman signal in Region 1, where the SWNT is exposed to air, to that in Region 3, where it is covered by graphene, also yields some interesting observations. Figure 5 shows the influence of the graphene on the RBM and G$^-$ peak position of the SWNT. In contrast to the G$^+$peak-position of the SWNT, the G$^-$-position can still be extracted from the Raman signal in Region 2 without the half-wave plate (i.e. the dark blue curve in Figure 2(c)). Figure 5 shows an upshift in

3. Discussion

The spectroscopic Raman data indicate that the graphene is being n-doped at the junction with the m-SWNT. Part of these electrons can come directly from the m-SWNT. When the SWNT and the graphene are brought in contact, electrons will flow from the material with more electrons (more shallow Fermi energy level E_F compared to vacuum) to the material
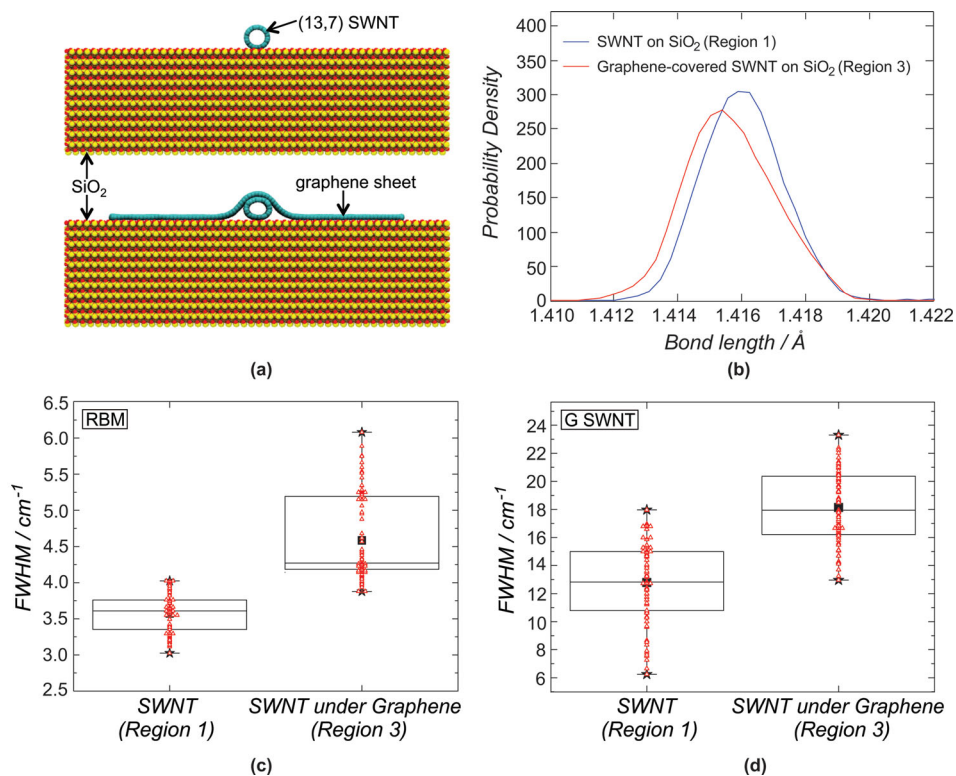

(a)

(b)

(c)

(d)

Figure 6. Influence of strain on the SWNT. (a) Molecular representation of the system (front view). Upper panel: (13,7) SWNT on SiO$_2$; lower panel: (13,7) SWNT on SiO$_2$ covered by a graphene sheet. (b) Distribution of bond lengths in the (13,7) SWNT. (a) Comparison of FWHM of the SWNT's RBM in Region 1 and Region 3. (d) Comparison of FWHM of the SWNT's G$^-$ peak in Region 1 and Region 3. The lower and higher ends of the boxplots represent the 25 and 75 percentile marks of the distributions respectively, and the middle line is the median value. Minimum and maximum values are represented by black stars, and the average is the black square. The red triangles in (c),(d) represent the complete dataset superimposed on the boxplots.

with fewer electrons (deeper E_F compared to vacuum) to equalize the Fermi levels in the two materials. The theoretical work function of SWNTs is chirality dependent. For a SWNT like the one studied by us with a diameter of ~1.35 nm, Barone et al. have calculated via density functional theory (DFT) that the work function is 4.5 eV, whereas the work function for graphene is determined to be 4.68 eV.[37] The work function is defined as the energy difference between the vacuum energy level and the Fermi energy (E_F) level of the material, which implies a material with a larger work function has a lower lying E_F (in this case graphene). Based on the DFT calculations of the work functions of the materials used in our study, we expect electrons to flow from the m-SWNT to the graphene, consistent with the doping trends observed in our Raman study. It should be noted that we use CVD-grown graphene that has been exposed to several processing steps during its growth and transfer, so it is likely that its work function deviates from a pristine graphene crystal lattice in vacuum.

The recorded Raman shifts can provide information about the amount of charge that is transferred between the m-SWNT and the graphene. Both Das et al.[29] and Farhat et al.[31,32] have studied Raman spectra of graphene and SWNT devices respectively under conditions of electrostatic doping. In the case of the former, Das et al. electrochemically gated a graphene monolayer with a polymer top gate (PEO/LiClO$_4$) and recorded the G-peak position shift as a function of the applied gate voltage V_G.[29] Farhat et al. gated a metallic SWNT with the same top gate (PEO/LiClO$_4$) and recorded both G-peak and RBM position shifts as a function of V_G.[31,32] Below, we calculate the carrier concentrations that correspond to the peak shifts in order to estimate the respective doping concentrations observed in SWNT/graphene junction reported in this work.

It is possible to relate V_G to the carrier concentration n and thus to relate typical Raman peak position shifts to added dopant concentrations:

$$for\ graphene:\ V_G = \frac{net_d}{\varepsilon\varepsilon_0} + \frac{\hbar v_{F,graphene}\sqrt{\pi n}}{e} \tag{1}$$
$$= An + B\sqrt{n}$$

$$for\ SWNT:\ V_G = \frac{ne\cosh^{-1}\left((t_d + r)/r\right)}{2\pi\varepsilon\varepsilon_0} + \frac{nhv_{F,SWNT}}{e} \tag{2}$$
$$= (C + D)n$$

where A, B, C and D are constants ≥ 0. In these equations e is the unit charge of an electron, t_d is the thickness of the dielectric, ε is the relative dielectric constant of the dielectric, ε_0 is the vacuum permittivity, h is the Planck constant and h_{bar} its reduced form, v_F is the Fermi velocity and r is the SWNT radius. The derivation of these equations is included in the Supporting Information (Section V).

Based on Das et al.'s recorded values of G peak shift vs. V_G,[29] and the relationship between V_G and n (Equation (1)) we deduce that a peak shift of about 10 cm^{-1} (observed in our own experiments in Figure S2(a))) requires a gate voltage of 1.2V which corresponds to an added electron concentration $\delta n = 1.12 \times 10^{13}$ cm^{-2}. Based on Farhat et al.'s recorded peak shifts of the RBM,[31] the shift we observe (~1.5 cm^{-1} (Figure 5(a))) requires at least a positive or negative gate voltage equal to |1.5 V|, which, according to Equation (2) implies a lower bound of the added electron or hole concentration of ~|δn| = 3.34 × 10^6 cm^{-1}. It should be noted that for both positive and negative applied gate voltages the observed RBM-shifts of the SWNT eventually saturate. The RBM position upshifts by ~ 1.5 cm^{-1} by applying a |V_G| = 1–1.5 V but for higher values of |V_G| the RBM peak position no longer changes (e.g. Figure 5 of ref. [31]). Our observed peak shift is located in this saturated region; hence we can only report a lower limit of the dopant concentration for the SWNT. Both p- and n-doping of the SWNT have a similar effect,[31,32] but since the graphene is being n-doped (electrons are added) on top of the SWNT, it is assumed the SWNT is being p-doped underneath the graphene (deprived of electrons).

Assuming a circular laser spot with a diameter of 1 μm (with an area of ~0.785 μm^2) during our Raman experiments, we can deduce the total amount of charge that is transferred per μm of SWNT. The graphene receives 8.792 × 10^3 electrons per μm of SWNT it covers, while the SWNT loses a minimum of 3.34 × 10^2 electrons per μm. It is plausible that part of the graphene n-doping is caused by the fact that the graphene on top of the SWNT is no longer in direct contact with the SiO$_2$, which is known to p-dope the graphene.[38] Some adsorbants on the SWNTs itself could potentially also cause additional doping, although we did anneal the SWNTs in air for 350 °C for 1.5 h to remove amorphous carbon and stored the SWNTs in a vacuum chamber until we put the graphene on top. When transferring the graphene to the wafer with SWNTs the junction is only exposed to deionized water, which then evaporates. Water has been shown to dope graphene.[39,40] Possibly some nanosize water clusters remain trapped between the SWNT and the graphene, which can locally dope the graphene. This again justifies the need for collecting many different spectra in order to get statistically significant results. Water molecules present in the air may also adsorb on the topside of the sample. This potentially causes a difference in the doping level of the SWNT in Region 1 versus the SWNT in Region 3.

We have examined the possibility that the close interaction between the SWNT lattice and the monolayer of polycrystalline graphene in Region 3 forms a structure resembling turbostratic graphene. Turbostratic graphene is characterized by a very different Raman signature than AB-stacked bilayer graphene or monolayer graphene.[41–43] Compared to pristine graphene both the 2D position, the 2D/G intensity ratio and the G peak width increase. In Region 3 (graphene on top of SWNT) we observe a downshift of the 2D peak compared to Region 2, a decrease of the 2D/G intensity ratio and a smaller G peak width. Therefore nothing points in the direction of a turbostratic monolayer/graphene SWNT interaction.

The amount of SWNT G band upshift with electrostatic gating is a matter of disagreement in the literature. Farhat et al. report an upshift of the G$^-$ peak of an m-SWNT by ~30 cm^{-1} upon the application of a polymer top gate voltage of |1.5 V| (the value of V_G that results in our observed upshift in RBM-peak);[32] whereas more modest upshifts of the G peak position of a SWNT upon doping are reported by others.[34–36]

In order for the G⁻ peak to upshift from ~1571 cm⁻¹ to 1575 cm⁻¹, as is the case in our data shown in Figure 5(b), a $V_G \cong |0.1\ V|$ is required, which implies a charge transfer of $0.223 \times 10^2\ \mu m^{-1}$, still within a factor of 15 of the previous analysis. According to Farhat et al. the G⁻ peak upshift we observe seems more typical for the observed upshift of the G⁺ peak of a m-SWNT or of the G-peak of a sc-SWNT.[32]

Radial compressive strain of the SWNT under the graphene sheet is another physical effect that can shift the RBM and G peak positions of SWNTs. A recent atomic force microscopy (AFM) study has shown a reduction of the height of a SWNT with an original diameter of 1.35 nm by nearly 23% when it is covered by a monolayer of graphene oxide (GO).[44]

While the effects of axial compression and strain on the SWNT Raman signal have been explored,[45,46] the effect of radial compression on the Raman spectrum of a single SWNT on a substrate has not yet been investigated. There is experimental and computational evidence for an upshift of the Raman peaks of SWNTs and SWNT bundles in solution under pressure.[47,48] The case of a single SWNT compressed by both the substrate underneath it and the graphene on top but free to expand sideways is likely different. Both molecular dynamics (MD) and experimental studies show the effect of axial strain and compression on the Raman peak positions of SWNTs is opposite: positive axial strain decreases peak positions whereas negative axial strain (compression) increases them.[45,46]

To estimate the amount of strain at equilibrium in our system (a sheet of monolayer graphene covering a (13,7) SWNT on SiO₂/Si substrate), we performed MD calculations at 300 K in the canonical (NVT) ensemble using the NAMD molecular dynamics package with CHARMM27 force-field parameters.[49,50] Our simulations were performed similarly to many other MD simulations of graphene and/or SWNT available in literature;[51–53] more details can be found in the Experimental Section. A visual representation of the SWNT on top of SiO₂ and graphene-covered SWNT on top of SiO₂ (generated with the VMD software package)[54] is shown in Figure 6(a); it is clear the graphene radially compresses the SWNT. Figure 6(b) shows the distribution of bond lengths in the SWNT before and after being covered by graphene and key results are summarized in **Table 1**.

The median of the bond length distribution is correlated to the Raman peak positions of the SWNT. Yang et al. performed calculations for axially strained SWNTs and showed that for a (10,10) m-SWNT (with very similar band structure to a (13,7) SWNT) the peak position (ω) changed with axial strain (ε) as:

Table 1. Key parameters of the bond length distribution of the SWNT in our system (with 95% confidence intervals).

	SWNT on SiO₂ [Å]	Graphene-covered SWNT on SiO₂ [Å]	Relative change [%]
Average	1.41589 ± 0.00004	1.41552 ± 0.00004	−0.03
Median	1.41600 ± 0.00004	1.41554 ± 0.00004	−0.03
FWHM	0.0017 ± 0.0003	0.0020 ± 0.0003	14.45

$$\frac{\partial \omega_{RBM}}{\partial \varepsilon} = -0.55 \frac{cm^{-1}}{\%} \qquad (3)$$

$$\frac{\partial \omega_{G^-}}{\partial \varepsilon} = -25.50 \frac{cm^{-1}}{\%} \qquad (4)$$

It should be noted this linear dependence is only true for small strains ($\sim|\varepsilon| < 2\%$).[45]

The Raman peak shifts caused by the graphene compressing the SWNT can be estimated as:

$$\begin{aligned} \Delta \omega_{RBM} &= \frac{\partial \omega_{RBM}}{\partial \varepsilon} \times \Delta \varepsilon \\ &= -0.55 \frac{cm^{-1}}{\%} \times -0.03\% = 0.0165\ cm^{-1} \end{aligned} \qquad (5)$$

$$\begin{aligned} \Delta \omega_{G^-} &= \frac{\partial \omega_{G^-}}{\partial \varepsilon} \times \Delta \varepsilon \\ &= -25.50 \frac{cm^{-1}}{\%} \times -0.03\% = 0.765\ cm^{-1} \end{aligned} \qquad (6)$$

where $\Delta \varepsilon$ is the relative change in the median value of the bond length distribution for the SWNT before and after coverage. From this analysis it is clear the observed (much larger) Raman peak shifts of the SWNT (Figure 5) can not be explained by strain and are thus caused by doping.

Further analysis revealed that although the average SWNT bond length does not change significantly when graphene covers it, about 58% of all the bonds are compressed (by ~−0.1%) and 42% are stretched (by ~0.07%) compared to the bond lengths of the SWNT on SiO₂ without graphene covering it. If we assume that the positive and negative bond strain have an opposite effect on the peak positions of the SWNT we can expect to see an inhomogeneous broadening of the RBM and G-peaks of the SWNT when covered by the graphene. This is confirmed by our Raman data. Figure 6(c) and (d) show that the FWHM for both the RBM and G⁻ peak of the SWNT increase by 27.7% (3.6 ± 0.3 to 4.6 ± 0.5 cm⁻¹) and 38.5% (13 ± 1 to 18 ± 1 cm⁻¹) respectively. The FWHM of the bond length distribution increases by 14.45% when the SWNT is covered by graphene, indicating that the strain and compression in the graphene-covered SWNT is largely responsible for the observed inhomogeneous broadening of its Raman peaks. It should be noted that Farhat et al. did not notice any significant change of the FWHM of the SWNT RBM and G-peaks upon doping.[31,32]

Graphene straining tends to downshift both its G peak and its 2D peak.[55] Mohiuddin et al. observe experimentally that applying less than 0.05% of uniaxial strain to SLG causes a downshift of the 2D peak position of ~3 cm⁻¹,[55] in agreement with the trend we observe (Figure 4(a)). However this is accompanied by a decrease of the G-peak position of ~5 cm⁻¹, whereas we observe an increase of ~10 cm⁻¹. Our observations of the effect of the SWNT on graphene can thus not be explained by strain. Moreover it would be surprising that graphene would be strained by a feature that is only 1.35 nm high; our MD simulations confirm that it is not (see Section VI of the Supporting Information). It is interesting to note that the persistence length of graphene at 300 K is calculated to be 5.5 nm.[56]

4. Conclusion

We have created a junction between a metallic SWNT and a single layer of graphene, both synthesized via CVD, and we have explored the electronic interactions between them. Raman spectroscopy in different regions of the sample allows for direct comparison between the spectra of graphene and SWNT individually with the spectra of the SWNT and the graphene where graphene covers the SWNT. The G peak position of the graphene upshifts when it covers the SWNT, a sign of charge transfer (doping), whereas its 2D peak position downshifts, which indicates it is being doped with electrons (n-type doping). A decreased 2D/G intensity ratio and G_{FWHM} confirm the trend. The RBM and G peak positions of the SWNT increase when it is covered by the graphene, again a sign of charge transfer. Based on this analysis we conclude the SWNT is being more p-doped under the graphene, and is thus n-doping the graphene. We calculate that a minimum electron density of ~334 μm^{-1} is transferred from the SWNT to the graphene. Based on the analysis of the G-peak upshift of the graphene, 8792 μm^{-2} electrons are donated to the graphene. With the help of a molecular dynamics simulation we deduce the effect of strain and radial compression on the Raman peak positions is limited and conclude that the Raman spectroscopic data indicate that the m-SWNT is donating electrons to the graphene.

5. Experimental Section

Cleaning of the SiO$_2$/Si Wafers: The SiO_2/Si wafers were cut with a die-saw (9 mm × 14 mm sample dimensions) and cleaned by ultrasonicating them for 10 min in acetone and for 10 min in IPA, after which they were dried with a stream of ultrapure N_2.

SWNT Growth: Aligned SWNTs were grown via atmospheric CVD on a SiO_2/Si (300 nm of SiO_2) wafer. The catalyst for growth is based on solution-dispersed SWNTs from Nano-C, grown with a pyrolysis method (Nano-CAPT). 2 mg/mL of the Nano-C SWNT were weighed out and added to a 2 wt% sodium cholate hydrate aqueous solution; the SWNTs were dispersed in the surfactant by homogenizing and tip-sonicating the mixture for 1 h each.

The solution typically contains about 30 wt% of Fe or Fe oxide nanoparticles. These Fe particles serve as the catalyst for the aligned SWNT growth, and the SWNTs already present in the catalyst disperse the particles such that many individual catalytic sites are present and such that the Fe-particles are now not necessarily stuck to the substrate, enabling lift-off from the surface during growth. The SWNTs 'float' along with the gas flow during growth; this mechanism is known as kite-growth.[57]

Using a syringe, a ~1mm wide strip of SWNT/Fe catalyst solution was deposited along the bottom edge of the SiO_2/Si wafer and the wafer was placed inside the quartz tube of the CVD furnace. The temperature is ramped up to 900 °C in 20 min under stable flow of 100 sccm ultrahigh-purity hydrogen (H_2), kept constant at 900 °C for 10 min, ramped up to 970 °C while flowing 3.4 sccm of H_2. At this point a stable flow of 2sccm ultrahigh-purity methane (CH_4) was added for the next 45 min during which the SWNTs grow.

After growth, the wafers with the SWNTs were annealed in air at 350 °C for 1.5 h to remove any possible amorphous carbon via oxidation.

Scanning electron microscopy imaging (SEM, model JEOL 6060) was used to verify SWNT growth and to identify the locations of suitably long SWNTs for detailed Raman characterization.

Graphene Growth and Transfer: SLG was synthesized by low-pressure CVD on a copper foil substrate (25 μm, 99.8%, Alfa Aesar) that acts as the catalyst. The Cu foil was cut (~3/4" × 2") and cleaned by submerging it in a 1:1 HCl:DI H_2O solution for 5 min, followed by rinsing it with DI H_2O, acetone and IPA. The film was then blow-dried with a N_2–gun and placed on a hotplate (85 °C) for 5 min. Under a stable H_2 flow (30 sccm), the Cu sheet was heated to 1000 °C in 20 min, and kept at 1000 °C for another 20 min to anneal it. Next, 3 sccm of CH_4 was added and graphene was synthesized for 35 min.

The graphene on Cu was covered in poly(methyl methacrylate) (950PMMA, A4, MicroChem) by spin coating (3000 rpm, 1 min) and dried in air (~15 min). Graphene on the reverse side of the Cu sheet was removed by reactive ion etching (Plasmatherm RIE, 100 W, 7 mtorr oxygen, 5 min). The Cu-graphene-PMMA stack was placed on the surface of Cu etchant (6 M HCl and 1 M $CuCl_2$ in water). After complete Cu etching (~30 min), the graphene-PMMA layer was scooped out with a clean wafer into several sequential baths of ultrapure water for rinsing. Finally it was scooped out with the target substrate (wafer with aligned SWNTs as described above) and dried in air overnight before immersion in several baths of clean acetone to dissolve the PMMA, followed by rinsing in isopropanol and drying with ultrapure nitrogen.

Raman: Raman spectroscopic measurements were performed on a Horiba Jobin Yvon LabRAM HR800 system using a 633 nm excitation laser, 100X objective lens with ~1 μm diameter spot size, and 600 lines/mm grating with ~3-4 cm^{-1} spectral resolution. The Raman peaks were fit to Lorentzians.

Molecular Dynamics Simulation: For the MD simulations VMD was used in combination with the NAMD package. For the SWNT and graphene the CHARMM27 force field was used,[49,50] and the VMD inorganic builder plugin was used to determine the SiO_2 force field.[54] The SiO_2 in the simulation is 50 unit cells long and wide (~25 nm), and 10 unit cells deep (~7 nm). The (13,7) SWNT (diameter ~1.35 nm) is 22 nm long. The graphene sheet covering the SWNT is 20 nm long and wide. The results of the simulation did not change significantly with the size of the simulated sample.

In the initial condition for the simulation the graphene sheet was bent into a Gaussian shape over the SWNT; the FWHM and height of the Gaussian were varied in several simulations to verify that the final equilibrated structure is independent of the initial conditions. It should be noted that when the graphene sheet was located too far from the SWNT at time 0, the structure did not converge to the same solution since in the simulation the VDW interactions were truncated after 12 Å. During the simulation the graphene and SWNT atoms were allowed to equilibrate and move, whereas the SiO_2 atoms remained fixed.

The simulations were run at 300 K (controlled via Langevin dynamics) in the NVT ensemble, assuming a vacuum and typically reach an equilibrium state after ~500 time steps (=1 ps). At first, each simulation was run for 15000 time steps. Then, the output coordinate file served as the initial condition for the next simulation and thermal velocities were redistributed. This was repeated 4 times. Out of each of those 4 simulations 500 time points were taken (in total 2000), which were then averaged.

Supporting Information

Acknowledgements

[1] K. S. Novoselov, A. K. Geim, S. V. Morozov, D. Jiang, M. I. K. I. V. Grigorieva, S. V. Dubonos, A. A. Firsov, *Nature* **2005**, *438*, 197.
[2] A. K. Geim, K. S. Novoselov, *Nat. Mater.* **2007**, *6*, 183.
[3] A. K. Geim, *Science* **2009**, *324*, 1530.
[4] M. S. Dresselhaus, G. Dresselhaus, P. C. Eklund, *Science of Fullerenes and Carbon Nanotubes*, Academic Press, Inc., San Diego, CA, USA **1996**.
[5] T. W. Odom, J. L. Huang, P. Kim, C. M. Lieber, *Nature* **1998**, *391*, 62.
[6] R. Saito, G. Dresselhaus, M. S. Dresselhaus, *Physical Properties of Carbon Nanotubes*, Imperial College Press, London, UK **1998**.
[7] Z. Yao, C. Dekker, P. Avouris, *Carbon Nanotubes* **2001**, *80*, 147.
[8] H. Cao, Q. Yu, L. A. Jauregui, J. Tian, W. Wu, Z. Liu, R. Jalilian, D. K. Benjamin, Z. Jiang, J. Bao, *Appl. Phys. Lett.* **2010**, *96*, 122106.
[9] J. C. Charlier, X. Blase, S. Roche, *Rev. Mod. Phys.* **2007**, *79*, 677.
[10] A. H. C. Neto, F. Guinea, N. M. R. Peres, K. S. Novoselov, A. K. Geim, *Rev. Mod. Phys.* **2009**, *81*, 109.
[11] S. Paulson, A. Helser, M. B. Nardelli, R. M. Taylor, M. Falvo, R. Superfine, S. Washburn, *Science* **2000**, *290*, 1742.
[12] T. Pei, H. Xu, Z. Zhang, Z. Wang, Y. Liu, Y. Li, S. Wang, L. M. Peng, *Appl. Phys. Lett.* **2011**, *99*, 113102.
[13] T. Yu, C. Kim, C. W. Liang, B. Yu, *IEEE Electron Device Lett.* **2011**, *32*, 1050.
[14] Y. C. Lin, C. Y. Lin, P. W. Chiu, *Appl. Phys. Lett.* **2010**, *96*, 133110.
[15] H. Liu, Y. Liu, D. Zhu, *J. Mater. Chem.* **2011**, *21*, 3335.
[16] T. O. Wehling, K. S. Novoselov, S. V. Morozov, E. E. Vdovin, M. I. Katsnelson, A. K. Geim, A. I. Lichtenstein, *Nano Lett.* **2008**, *8*, 173.
[17] L. S. Panchakarla, K. S. Subrahmanyam, S. K. Saha, A. Govindaraj, H. R. Krishnamurthy, U. V. Waghmare, C. N. R. Rao, *Adv. Mater.* **2009**, *21*, 4726.
[18] I. Gierz, C. Riedl, U. Starke, C. R. Ast, K. Kern, *Nano Lett.* **2008**, *8*, 4603.
[19] Q. H. Wang, J. Zhong, K. K. Kim, A. J. Hilmer, G. L. C. Paulus, C.-J. Shih, M.-H. Ham, J. Sanchez-Yamagishi, K. Watanabe, T. Taniguchi, J. Kong, P. Jarillo-Herrero, M. S. Strano, *Nat. Chem.* **2012**, *4*, 724.
[20] M. S. Dresselhaus, G. Dresselhaus, R. Saito, A. Jorio, *Phys. Rep.* **2005**, *409*, 47.
[21] A. Jorio, P. T. Araujo, S. K. Doorn, S. Maruyama, H. Chacham, M. A. Pimenta, *Phys. Status Solidi B* **2006**, *243*, 3117.
[22] A. C. Ferrari, J. C. Meyer, V. Scardaci, C. Casiraghi, M. Lazzeri, F. Mauri, S. Piscanec, D. Jiang, K. S. Novoselov, S. Roth, *Phys. Rev. Lett.* **2006**, *97*, 187401.
[23] A. C. Ferrari, *Solid State Commun.* **2007**, *143*, 47.
[24] G. S. Duesberg, I. Loa, M. Burghard, K. Syassen, S. Roth, *Phys. Rev. Lett.* **2000**, *85*, 5436.
[25] A. Jorio, A. G. Souza Filho, V. W. Brar, A. K. Swan, M. S. Ünlü, B. B. Goldberg, A. Righi, J. H. Hafner, C. M. Lieber, R. Saito, *Phys. Rev. B* **2002**, *65*, 121402.
[26] J. Hwang, H. H. Gommans, A. Ugawa, H. Tashiro, R. Haggenmueller, K. I. Winey, J. E. Fischer, D. B. Tanner, A. G. Rinzler, *Phys. Rev. B* **2000**, *62*, 13310.
[27] C. Casiraghi, S. Pisana, K. S. Novoselov, A. K. Geim, A. C. Ferrari, *Appl. Phys. Lett.* **2007**, *91*, 233108.
[28] C. Casiraghi, *Phys. Rev. B* **2009**, *80*, 233407.
[29] A. Das, S. Pisana, B. Chakraborty, S. Piscanec, S. K. Saha, U. V. Waghmare, K. S. Novoselov, H. R. Krishnamurthy, A. K. Geim, A. C. Ferrari, *Nat. Nanotechnol.* **2008**, *3*, 210.
[30] S. Pisana, M. Lazzeri, C. Casiraghi, K. S. Novoselov, A. K. Geim, A. C. Ferrari, F. Mauri, *Nat. Mater.* **2007**, *6*, 198.
[31] H. Farhat, K. Sasaki, M. Kalbac, M. Hofmann, R. Saito, M. S. Dresselhaus, J. Kong, *Phys. Rev. Lett.* **2009**, *102*, 126804.
[32] H. Farhat, H. Son, G. G. Samsonidze, S. Reich, M. S. Dresselhaus, J. Kong, *Phys. Rev. Lett.* **2007**, *99*, 145506.
[33] L. Kavan, M. Kalbác, M. Zukalová, L. Dunsch, *J. Phys. Chem. B* **2005**, *109*, 19613.
[34] K. T. Nguyen, A. Gaur, M. Shim, *Phys. Rev. Lett.* **2007**, *98*, 145504.
[35] A. Z. Hartman, M. Jouzi, R. L. Barnett, J. M. Xu, *Phys. Rev. Lett.* **2004**, *92*, 236804.
[36] M. Stoll, P. Rafailov, W. Frenzel, C. Thomsen, *Chem. Phys. Lett.* **2003**, *375*, 625.
[37] V. Barone, J. E. Peralta, J. Uddin, G. E. Scuseria, *J. Phys. Chem.* **2006**, *124*, 024709.
[38] Y. J. Kang, J. Kang, K. J. Chang, *Phys. Rev. B* **2008**, *78*, 115404.
[39] K. T. He, J. D. Wood, G. P. Doidge, E. Pop, J. W. Lyding, *Nano Lett.* **2012**, *12*, 2665.
[40] P. Cao, J. O. Varghese, K. Xu, J. R. Heath, *Nano Lett.* **2012**, *12*, 1459.
[41] K. Kim, S. Coh, L. Z. Tan, W. Regan, J. M. Yuk, E. Chatterjee, M. F. Crommie, M. L. Cohen, S. G. Louie, A. Zettl, *Phys. Rev. Lett.* **2012**, *108*, 246103.
[42] Z. Ni, Y. Wang, T. Yu, Y. You, Z. Shen, *Phys. Rev. B* **2008**, *77*, 235403.
[43] K. Kim, Z. Lee, B. D. Malone, K. T. Chan, B. Alemán, W. Regan, W. Gannett, M. F. Crommie, M. L. Cohen, A. Zettl, *Phys. Rev. B* **2011**, *83*, 245433.
[44] M. Zheng, L. Zou, H. Wang, C. Park, C. Ke, *ACS Nano* **2012**, *6*, 1814.
[45] W. Yang, R. Z. Wang, H. Yan, *Phys. Rev. B* **2008**, *77*, 195440.
[46] S. B. Cronin, A. K. Swan, M. S. Ünlü, B. B. Goldberg, M. S. Dresselhaus, M. Tinkham, *Phys. Rev. B* **2005**, *72*, 035425.
[47] U. Venkateswaran, A. Rao, E. Richter, M. Menon, A. Rinzler, R. Smalley, P. Eklund, *Phys. Rev. B* **1999**, *59*, 10928.
[48] I. Loa, *J. Raman Spectrsc.* **2003**, *34*, 611.
[49] J. C. Phillips, R. Braun, W. Wang, J. Gumbart, E. Tajkhorshid, E. Villa, C. Chipot, R. D. Skeel, L. Kale, K. Schulten, *J. Comput. Chem.* **2005**, *26*, 1781.
[50] A. D. MacKerell Jr., D. Bashford, R. L. Dunbrack, J. D. Evanseck, M. J. Field, S. Fischer, J. Gao, H. Guo, S. Ha, D. Joseph-McCarthy, L. Kuchnir, K. Kuczera, F. T. K. Lau, C. Mattos, S. Michnick, T. Ngo, D. T. Nguyen, B. Prodhom, W. E. Reiher, B. Roux, M. Schlenkrich, J. C. Smith, R. Stote, J. Straub, M. Watanabe,

J. Wiórkiewicz-Kuczera, D. Yin, M. Karplus, *J. Phys. Chem. B* **1998**, *102*, 3586.

[51] N. Patra, B. Wang, P. Král, *Nano Lett.* **2009**, *9*, 3766.

[52] E. P. Bellido, J. M. Seminario, *J. Phys. Chem. C* **2010**, *114*, 22472.

[53] N. Patra, Y. Song, P. Král, *ACS Nano* **2011**,

[54] W. Humphrey, A. Dalke, K. Schulten, *J. Mol. Graphics* **1996**, *14*, 33.

[55] T. M. G. Mohiuddin, A. Lombardo, R. R. Nair, A. Bonetti, G. Savini, R. Jalil, N. Bonini, D. M. Basko, C. Galiotis, N. Marzari, *Phys. Rev. B* **2009**, *79*, 205433.

[56] M. Neek-Amal, R. Asgari, M. R. Rahimi Tabar, *Nanotechnology* **2009**, *20*, 135602.

[57] C. Lu, Q. Fu, S. Huang, J. Liu, *Nano Lett.* **2004**, *4*, 623.

[58] D. M. Basko, S. Piscanec, A. C. Ferrari, *Phys. Rev. B* **2009**, *80*, 165413.